Supporting Information: Methanol and Ammonia as Emerging Green Fuels: Evaluation of a New Power Generation Paradigm

Elena C. Blanco [1], Antonio Sánchez [1], Mariano Martín [1], Pastora Vega [2]

[1] Department of Chemical Engineering, University of Salamanca, 37008 Salamanca, Spain

[2] Department of Computer Science, University of Salamanca, 37008 Salamanca, Spain

1 Process description

Figures S1 -S4 show the process flow diagram for each of the ammonia and methanol alternatives.

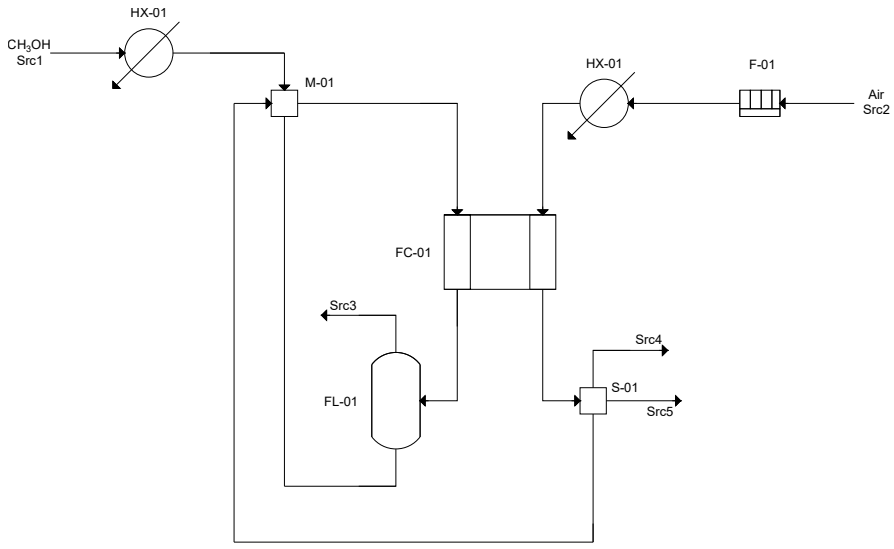

Figure S1: Process flow diagram of the electrochemical route of methanol.

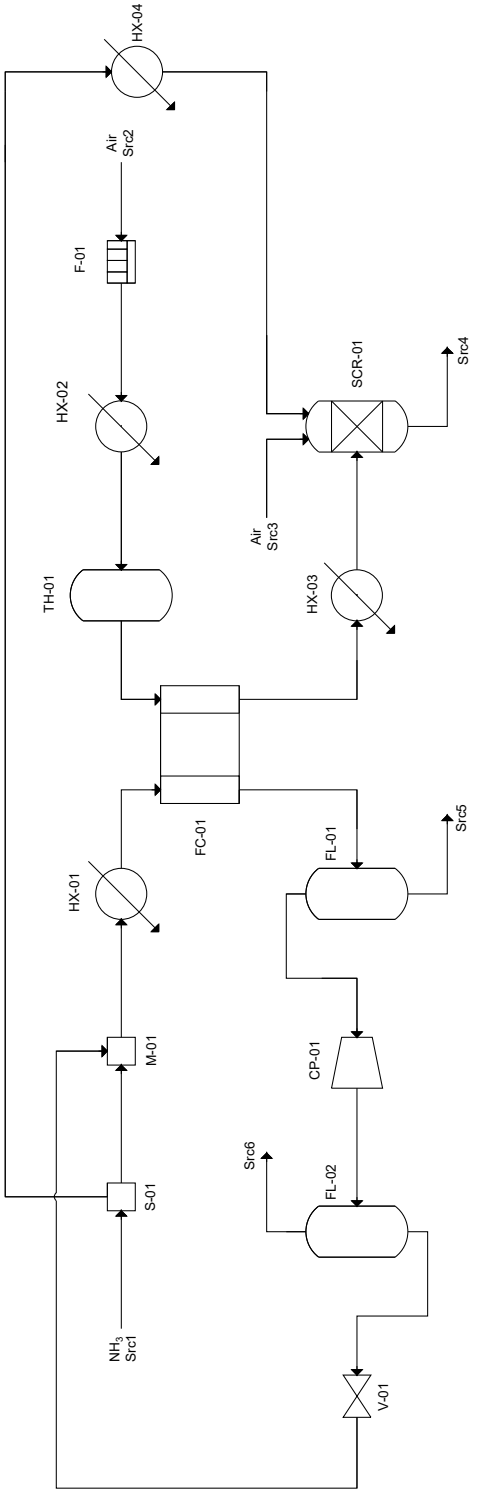

Figure S2: Process flow diagram of the electrochemical route of ammonia.

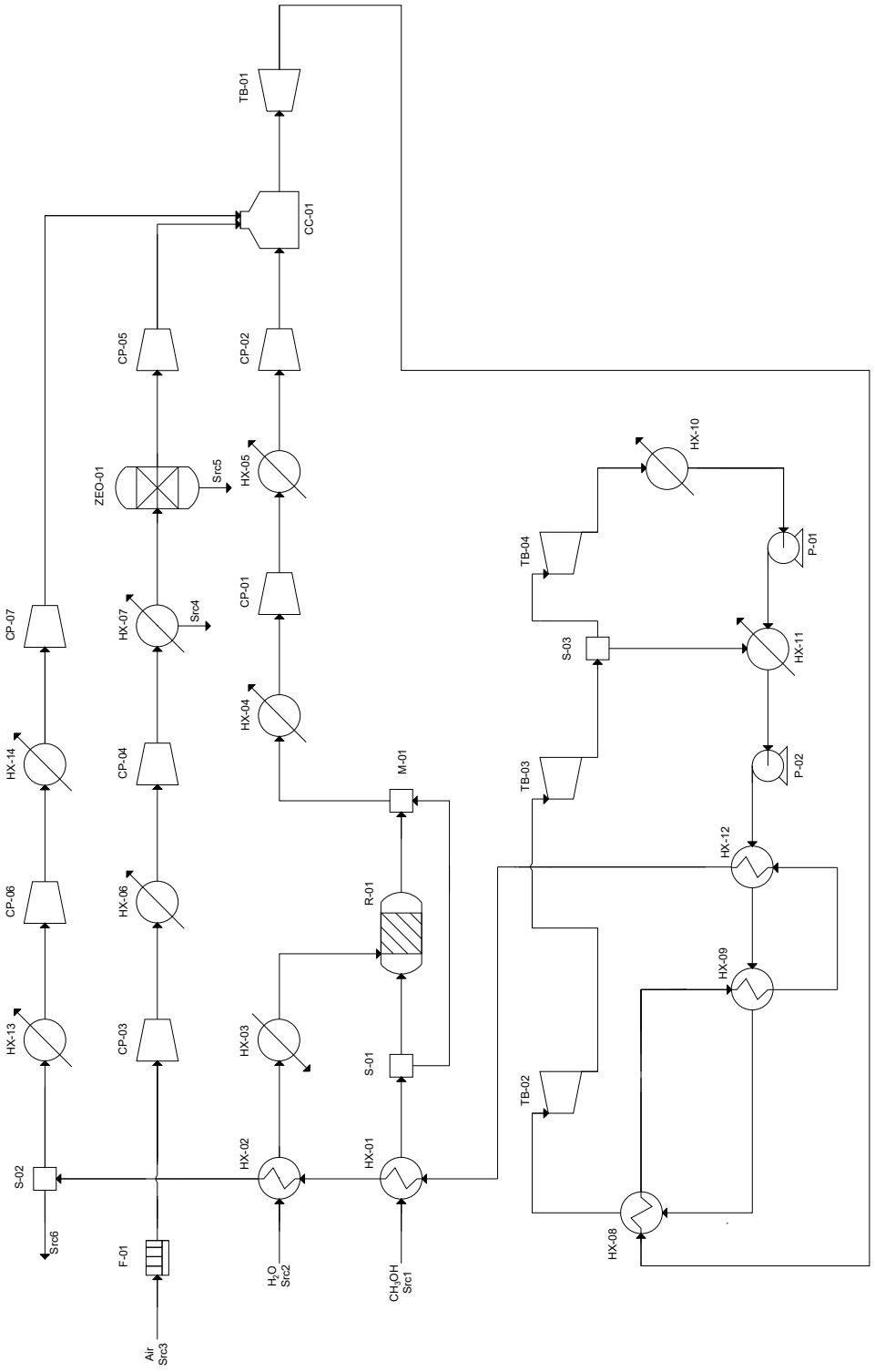

Figure S3: Process flow diagram of the termochemical route of methanol.

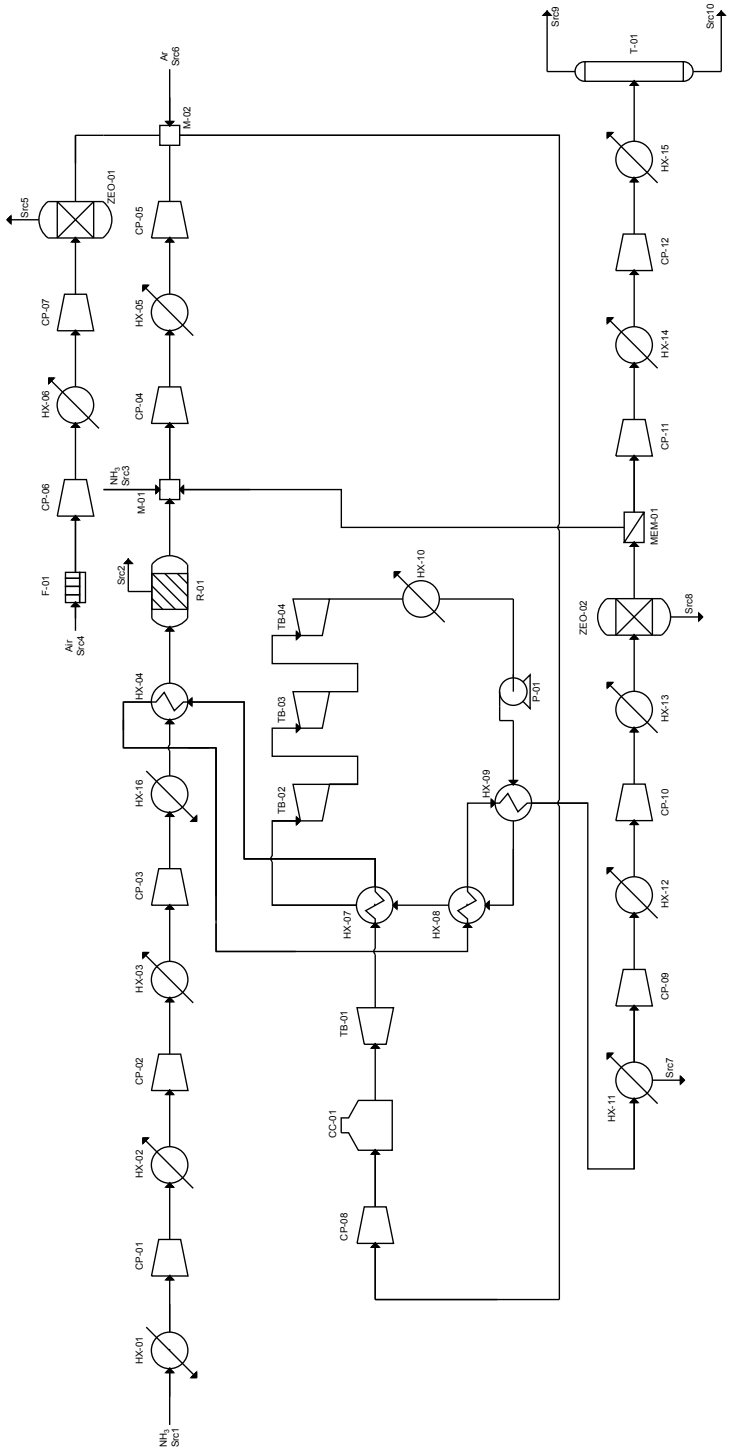

Figure S4: Process flow diagram of the termochemical route of ammonia.

2 Modeling approach

In this section, the modeling approach used in the different sections of the process of conversion of methanol/ammonia into power is explained.

2.1 Thermochemical route

2.1.1 Feedstock preparation

For the case of methanol, the use of a steam reforming unit is introduced to produce the necessary hydrogen for the combustion of methanol. In this reactor, three main reactions are involved: the methanol steam reforming reaction (Eq.S1), the water gas shift reaction (Eq.S2), and the methanol decomposition reaction (Eq.S3).

$$CH_3OH + H_2O \rightleftharpoons CO_2 + 3H_2 \tag{S1}$$

$$CO + H_2O \rightleftharpoons CO_2 + H_2 \tag{S2}$$

$$CH_3OH \rightleftharpoons CO + 2H_2 \tag{S3}$$

These reactions occur in a fixed-bed catalytic reactor with $Cu/ZnO/Al_2O_3$ as catalyst due to its good catalytic activity, fast kinetic, high selectivity, and low cost (Zhu et al., 2020). The inlet temperature of this unit is between 473-573 K and 1-5 atm with a steam to methanol ratio between 1:1 and 3:1 (Ghasemzadeh et al., 2020). As the rate-limiting step of the methanol decomposition mechanism is the adsorption over the catalytic surface, the kinetic model is based on a Langmuir-Hinshelwood expression and, in this work, is taken from Peppley et al. (1999). To include the reactor model in the superstructure optimization, a surrogate model was created. In a first step, a rigorous model based on a set of differential equations is developed to describe the performance of the decomposition reactor (as shown in Section 3). In a second step, a surrogate model is created to describe the performance of the reactor from the results of the previous step. In the presented model, the conversion (X_{reac}) reached in the unit is a function of the inlet pressure (P in atm, between 1-5 atm) and temperature (T in K, between 473-573 K) of the reactor, the inlet gas velocity (v_{reac} in m/s, between 1-3 m/s) and the inlet ratio between water and methanol (r, between 1-3) as it is shown in Eq.S4.

$$\begin{aligned} X_{reac} = {} & -5.99 - 0.130P + 0.0187T - 0.139v_{reac} + 0.057r + 0.0120P^2 \\ & - 0.00011T^2 + 0.0183v_{reac}^2 - 0.0308r^2 + 0.000026PT - 0.00607Pv_{reac} \\ & + 0.00331Pr + 0.000021Tv_{reac} + 0.000116Tr + 0.0031v_{reac}r \end{aligned} \tag{S4}$$

In the case of ammonia, an ammonia decomposition reactor is introduced to produce the hydrogen required to prepare the fuel blend. The ammonia decomposition reaction is as follows:

$$NH_3 \rightleftharpoons \frac{1}{2}N_2 + \frac{3}{2}H_2 \tag{S5}$$

This reaction is carried out in a fixed-bed catalytic membrane reactor. The selected catalyst is Ni/Al_2O_3 with a good catalytic performance and where Ni is widely accepted as an economical alternative to ruthenium catalyst (Chiuta et al., 2013). A H_2 selective membrane is installed in the reactor to separate hydrogen in the same unit and to improve the conversion of the reactor. A Pd-Ag supported membrane is widely accepted for these purposes (Cechetto et al., 2021). The kinetic expression for this ammonia decomposition is adapted from the Temkin equation (Kim et al., 2018) and the rate of permeation of hydrogen is based on the gradient of partial pressure on both sides of the membrane (Abashar, 2018) (as shown in Section 3). As in methanol reforming, a surrogate model is created to include the rigorous formulation in the optimization analysis. In this model, the conversion (Eq.S6) of the reactor is calculated as a function of the inlet temperature (T in K, between 700-850K) and pressure (P in atm, between 10-50 bar), the inlet gas velocity (v_{reac} in m/s, between 0.85-1.5 m/s), and the total recovery of hydrogen in the unit (X_{total}, between 0.85-0.95) (Sánchez et al., 2021).

$$\begin{aligned} X_{reac} = &-2.305 - 0.0060P + 0.0051T + 0.0010v_{reac} + 2.744X_{total} \\ &- 1.424 \times 10^{-6}T^2 + 3.884 \times 10^{-6}PT + 0.0040PX_{total} - 0.0033TX_{total} \end{aligned} \tag{S6}$$

2.1.2 Energy conversion

The transformation of methanol/ammonia into electricity via the thermochemical route is based on a combined cycle in both cases. The first step in this conversion is a gas turbine. This unit is modeled using three different sections: a multistage compression step, the combustion chamber, and the expansion into a turbine to produce power (León and Martín, 2016). For the compression and expansion stages, a polytropic process is assumed with a polytropic coefficient (k) equal to 1.4 and an efficiency of 0.85. For the combustion of methanol, a blend consisting of 85% of methanol and 15% of hydrogen is introduced into the chamber (Zhen and Wang, 2015). The amount of air to be introduced is based on the global excess air ratio. The typical range for methanol combustion is around 1.2-1.5, with a value of 1.2 selected in this work based on good results for this value in the literature (Zhang et al., 2015). The combustion of methanol could reach high temperature values, above 1600ºC, proposed as the maximum level for the current gas turbines systems. To control the temperature of the combustion chamber, a fraction of the flue gases is recycled to limit the temperature of the unit. Nitrogen oxide emerges as the main pollutant in the combustion of methanol. The amount of this component in the exhaust gases from the combustion is calculated as a function of the hydrogen concentration of the inlet mixture (as explained in Section 4) (Gong et al., 2016).

In the case of ammonia, the amount of air to be introduced is computed as a function of the equivalent ratio (ER). The ER is limited within the experimental range of 1.2-1.4 (Khateeb et al., 2020). The maximum temperature of the gas turbine is 1600ºC, controlling this value by means of an inert (argon) (Duynslaegher et al., 2009; Sánchez et al., 2021). The main gases leaving the combustion chamber are nitrogen, water, oxygen, hydrogen, and the inert component to control the temperature. Additionally, one of the main challenges in the combustion of ammonia is the formation of nitrogen oxides. The amount of this pollutant is computed

using an empirical correlation where the concentration is a function of the ER (as explained in Section 4) (Valera-Medina et al., 2019). In both cases (methanol and ammonia), the combustion performance (including gas composition and final temperature) is calculated using mass and energy balances, and different equations based on experimental results.

The last part of this energy conversion section is the Rankine cycle. The hot gases from the gas turbine produce steam which is used to generate power in a steam turbine system increasing the energy efficiency of the process. In both cases, three different turbines (high, medium, and low pressure) are introduced to model the multistage expansion of a real steam turbine. The high pressure steam turbine operates with an inlet pressure between 95-125 bar, the medium pressure between 11-35 bar, and the low pressure in the range of 5-9.5 bar. A thermodynamic approach is followed to describe the performance of the Rankine cycle with reheat. The enthalpies and entropies of the different steam streams are calculated from the correlations proposed by León and Martín (2016) using experimental data. The isoentropic efficiency of each of the turbines is fixed to 0.9 (Sadi and Arabkoohsar, 2019).

2.1.3 Gas cleanup

The gases from the combustion section may contain some valuable components such as hydrogen or, in addition, a pollutant may be generated during the burning of the liquid fuel. These gases must be treated to recover the specific components that can be recycled and to remove the pollutants to comply with the environmental restrictions.

For methanol combustion, the main constituents of the gas stream are carbon dioxide and water from the combustion and, also, oxygen and nitrogen from the inlet air. After the energy conversion section, a fraction of these gases is recycled to the fuel blend preparation to reduce the temperature of the gas turbine during methanol combustion. But, no further treatment is required for this stream.

When ammonia is used as fuel, two components that require attention appear in the combustion gases: nitrogen oxides and hydrogen. The concentration of NO_x is below the legally permitted limit, therefore, no specific treatment is required (Sánchez et al., 2021). Hydrogen is a valuable component that has to be recovered from the outlet stream to reintroduce it into the combustion section. A hydrogen selective membrane is adopted in this work with a hydrogen separation factor equal to 68 (Zhu et al., 2017). The operating pressure of this unit is 6 bar. After that, the outlet stream is constituted, mainly, of nitrogen (from ammonia combustion and from the inlet air) and argon (introduced as an inert component in the ammonia combustion). These two components are separated using a cryogenic distillation system operating in the range of 40-60 bar. The modeling is based on mass and energy balances, however, some surrogate models from the rigorous simulation (using CHEMCAD) are introduced to compute the temperature and gas fraction after the gas expansion (Sánchez et al., 2021).

2.2 Electrochemical route

2.2.1 Fuel cell operation

In the case of direct methanol fuel cells (DMFCs), methanol is oxidized in the presence of water at the anode, generating carbon dioxide, protons, and electrons according to the reaction in Eq.S7. These protons cross the membrane electrolyte to the cathode, while the electrons pass there through an external circuit to produce electricity, and both react with the oxygen in the air to generate water according to the reaction in Eq.S8.

$$CH_3OH + H_2O \rightarrow CO_2 + 6\,H^+ + 6\,e^- \tag{S7}$$

$$6\,H^+ + 6\,e^- + \frac{3}{2}\,O_2 \rightarrow 3\,H_2O \tag{S8}$$

The overall reaction is (Li and Faghri, 2013):

$$CH_3OH + \frac{3}{2}\,O_2 \rightarrow CO_2 + 2\,H_2O \tag{S9}$$

The amount of fuel fed into a fuel cell depends on the fuel cell efficiency. This efficiency is the ratio of the amount of power obtained in the fuel cell (W) to the total energy that can be obtained from the fed fuel (n) as a function of its lower heating value (LHV) (Eq.S10).

$$\varepsilon = \frac{W}{n \cdot LHV} = \frac{p \cdot A}{n \cdot LHV} = \frac{E \cdot j \cdot A}{n \cdot LHV} \tag{S10}$$

The generated power is the product of the power density (p) and the active area of the fuel cell (A). The active area of the cell is set to 780 cm^2/cell in this work (Yürüm, 2013). The power density in the fuel cell depends on the operating voltage (E) and current density (j). These two variables are related by the polarization curves, and in this work, a experimental model (following the methodology proposed by Schulze Lohoff et al. (2016)) is obtained. This model (Eq.S11) has been obtained by considering the experimental data of Zhang and Liu (2009) taking into account that the current density (j_{CH_3OH}) is between 0-0.48 A/cm^2 in this case.

$$E_{CH_3OH} = -1.177 \cdot j_{CH_3OH}^3 + 4.632 \cdot j_{CH_3OH}^2 - 1.883 \cdot j_{CH_3OH} + 0.633 \tag{S11}$$

The current delivered by a fuel cell is directly proportional to the amount of fuel consumed to produce energy (n) because each mole of fuel provides the corresponding moles of electrons, following Faraday's law (Eq.S12). This equation also allows to calculate the consumed flow rates of the other chemicals in the fuel cell by considering the number of electrons (n_e) in each reaction (Eq.S7 and Eq.S8), and, therefore, to calculate the output flow rates.

$$j = n_{fc} \cdot n_e \cdot F \tag{S12}$$

In addition to the fuel consumed by the electrochemical reaction, a fraction of the fed fuel is consumed not producing energy since it crosses the membrane and is oxidized at the cathode

following the reaction given at Eq.S13. This is called "crossover".

$$CH_3OH + \frac{3}{2} O_2 \rightarrow CO_2 + 2\,H_2O \tag{S13}$$

The methanol crossover can be obtained as a function of the operating current density (j) following the experimental data of Zhang and Liu (2009) (Eq.S14) considering, as an indicator, the hypothetical current density of the methanol passing through the membrane ($j_{xover_{CH_3OH}}$). In Eq.S14, the current density is specified in A/cm^2 and the range of j is between 0-0.48 A/cm^2.

$$j_{xover_{CH_3OH}} = -0.1697 \cdot j + 0.1039 \tag{S14}$$

In the case of methanol, it must be considered that there is an amount of water crossing the membrane from the anode to the cathode which is called electro-osmotic water drag. The flux of drag water can be calculated according to Eq.S15, as a function of the current density (Zenith and Krewer, 2010).

$$N_d = k_d \cdot \frac{j}{F} \tag{S15}$$

Where k_d is a constant value that depends on the operating temperature of the fuel cell, that, in this work, it is set to 333 K. This relationship is collected in equation Eq.S16 where the temperature is measured in K.

$$k_d = 4.2 + \frac{(T - 303.15)}{40} \tag{S16}$$

This water transport can also include methanol, but, in this case, it is not considered because it is less important than methanol crossover due to the low concentration of the solution (Zenith and Krewer, 2010).

In the case of direct ammonia fuel cells (DAFCs), ammonia reacts with hydroxyl ions at the anode to produce nitrogen, water, and electrons according to the reaction in Eq.S17. As in the case of methanol, electrons pass to the cathode via an external circuit, producing electricity. At the cathode, water reacts with the electrons and oxygen, generating hydroxyl ions that cross the membrane electrolyte towards the anode according to the reaction in Eq.S18. The overall reaction can be seen in Eq.S19 (Dincer and Siddiqui, 2020).

$$2\,NH_3 + 6\,OH^- \rightarrow N_2 + 6\,H_2O + 6\,e^- \tag{S17}$$

$$\frac{3}{2} O_2 + 6\,e^- + 3\,H_2O \rightarrow 6\,OH^- \tag{S18}$$

$$2\,NH_3 + \frac{3}{2} O_2 \rightarrow N_2 + 3\,H_2O \tag{S19}$$

As in the case of methanol, the amount of fuel fed into a fuel cell depends on the fuel cell efficiency (Eq.S10). Also, a experimental model (Eq.S20) is obtained to relate the voltage (E_{NH_3}) and the current density (j_{NH_3}) considering the experimental data of Achrai et al. (2020). In this equation, the operating voltage is expressed in V and the current density in A/cm^2,

taking into account that the current density is between 0-0.44 A/cm^2.

$$E_{NH_3} = -398.1 \cdot j_{NH_3}^5 + 499.53 \cdot j_{NH_3}^4 - 233.89 \cdot j_{NH_3}^2 + 50.117 \cdot j_{NH_3}^2 - 5.4094 \cdot j_{NH_3} + 0.6207 \tag{S20}$$

The current delivered by the ammonia fuel cells is also directly proportional to the amount of ammonia consumed to produce energy, also following Faraday's law (Eq.S12). The consumed flow rates of the other chemicals in the fuel cell can be calculated by this equation, considering the number of electrons in each reaction (Eq.S17 and Eq.S18), and, therefore, the output flow rates can be also obtained.

There is also a fraction of the fed ammonia that is oxidized at the cathode but not producing energy following the reaction given at Eq.S21.

$$2\,NH_3 + \frac{5}{2}\,O_2 \rightarrow 2\,NO + 3\,H_2O \tag{S21}$$

The ammonia crossover is estimated to be approximately 20% of the amount of ammonia consumed in the electrochemical reaction (Cha et al., 2009).

For both cases, the stoichiometry of the reactions in Eq.S9 and Eq.S19 allows calculating the amount of air to be fed into the fuel cells, considering that its composition is 79/21 nitrogen to oxygen and that it has a relative humidity of 72% (at ambient temperature). In the case of ammonia, it is necessary to increase the amount of water contained in the air, before it is fed to the cathode, for the reaction to take place. Considering that the relative humidity of the air must be 50% after the humidifier at 368 K, the neccesary amount of water and air must be introduced into the fuel cell (Siddiqui and Dincer, 2019).

Finally, the amount of fuel that is introduced, but not converted into power, generates heat that must be removed by the cooling water to maintain the isothermal operation of the fuel cell. The amount of energy transferred to the water can be estimated by the Eq.S22, taking into account the lower heating value of the fuel (LHV), the fuel cell efficiency (ε) and assuming an overall heat loss in the transfer process (ν) of 10%.

$$Q = n \cdot LHV \cdot (1 - \varepsilon - \nu) \tag{S22}$$

2.2.2 Gas cleanup

In the case of methanol, water consumption is lower than water production, so it is possible to recirculate it from the cathode outlet to the anode inlet, reducing the net consumption (Li and Faghri, 2013). It is possible to recirculate the liquid methanol and water from the anode outlet to the anode inlet, as they are not consumed at all (Lee et al., 2017). For this purpose, a flash distillation is used considering that the gaseous carbon dioxide, which also leaves the anode, is completely separated from the methanol and water. To obtain the amount of water to be separated from the cathode outlet, it is necessary to consider the amount of methanol that is introduced (Eq.S10), since it is fed to the fuel cell as an aqueous solution with 1 M concentration, and the amount of water leaving the anode. After separating the necessary

water, the remaining components of the cathode output (oxygen, nitrogen, water, and carbon dioxide) are released (Na et al., 2015).

In the case of ammonia, air, nitrogen, water, and nitrogen monoxide are obtained at the cathode outlet. This output stream is sent to a selective catalytic reduction system to remove nitrogen monoxide using ammonia and air according to the reaction given in Eq.S23.

$$4\,NO\ +\ 4\,NH_3\ +\ O_2\ \rightarrow\ 4\,N_2\ +\ 6\,H_2O \tag{S23}$$

It is necessary to introduce more ammonia than the amount computed from the efficiency equation (S10). Before introducing it into the treatment system, it is necessary to increase the temperature of the stream to the operating temperature of the system, 545-640 K. Besides that, ammonia is fed to the system with an excess of 5% over the stoichiometric amount in the reaction, and air, with a relation of 20:1 to ammonia, to work within the flammability limits. In this work, a removal efficiency of 99.9% is assumed (Guerras and Martín, 2019). Finally, the anode output stream, which contains unreacted ammonia, water, and nitrogen is separated using a sequence of two flash units to be able to recycle the ammonia to the fuel cell. The nitrogen stream could be recycled to the ammonia synthesis section avoiding the loss of this valuable component.

2.3 Optimization procedure

The transformation of methanol/ammonia into power has been formulated as a set of nonlinear programming (NLP) problems, one per each of the alternatives evaluated. Using different modeling approaches the problem is able to optimize the operating conditions in the facility. Therefore, for a given power production capacity, the optimization problem determines the best values of the operating variables (temperature, pressure, ratios, etc.) to produce the required power from methanol/ammonia considering the entire facility as a whole. As objective function of this optimization problem, a simplified form of the operating cost of the facility is considered:

$$obj = \sum_{i \epsilon IN} f_i C_i - \sum_{j \epsilon OUT} f_j C_j \tag{S24}$$

where f_i is the inlet/outlet flow of the different resources involved in the process and C_i the cost associated with each of the resources. One of the main parameters that determine the operating cost of the facility is the price of methanol/ammonia, the main raw materials. As a base case scenario, the price of methanol is set to \$518/t and the price of ammonia to \$662.9/t (Matzen et al., 2015b). Using the same source for the prices of methanol and ammonia, a fair comparison of both chemicals can be performed in terms of power production. Other prices for the inlet/outlet resources included in the optimization have been: for N_2, 0.037 €/kg (Elishav et al., 2017), for Ar, 0.5 €/kg (Downie, 2007), for H_2, 4 €/kg (Matzen et al., 2015a).

The problem is implemented in GAMS solving the NLP problem for each of the alternatives using a multistart optimization methodology with CONOPT 3.0 as preferred solver. After the

optimization procedure, and using the data from it, an assessment of the energy performance of the system is performed together with an economic analysis of the different facilities. Further details on the economic analysis are provided in Table S4 and in Section 6. During the scale-up analysis, some of the units involved must be duplicated because the maximum level is reached. This behavior is included during the economic evaluation of the process.

3 Reactor models

3.1 Ammonia membrane reactor

In the decomposition membrane reactor, ammonia is converted to nitrogen and hydrogen, according to the reaction S25, and this component passes through the membrane and is separated in situ.

$$NH_3 \rightleftharpoons \frac{1}{2} N_2 + \frac{3}{2} H_2 \tag{S25}$$

The catalyst used in the decomposition section is Ni/Al_2O_3 and a Pd-Ag supported membrane is installed to recover the hydrogen from the decomposition of ammonia. The kinetics expression of the ammonia decomposition reaction is adapted from the Temkin expression (Kim et al., 2018; Dyson and Simon, 1968):

$$r = 3k_{reac}\left[K_p^2 a_{N_2}\left(\frac{a_{H_2}^3}{a_{NH_3}^2}\right)^{\alpha} - \left(\frac{a_{NH_3}^2}{a_{H_2}^3}\right)^{1-\alpha}\right]\Phi\Omega \tag{S26}$$

Where k_{reac} is the kinetic constant of the reaction, K_p is the equilibrium constant, a_i is the activity of component i, Φ is the effectiveness factor, Ω is the catalytic activity and α is a kinetic parameter. To describe the permeation through the membrane, the following expression (S27) is introduced using the gradient of pressure on both sides of the membrane as driving force (Abashar, 2018).

$$r_{H_2}^p = \left(\frac{28.84 \cdot 10^{-5}}{\delta}\right) exp\left(\frac{-1888.381}{T}\right)\left(\sqrt{P_{H_2}^r} - \sqrt{P_{H_2}^p}\right) \tag{S27}$$

Where δ is the thickness of the membrane, T is the reactor temperature and $P_{H_2}^j$ is the partial pressure of hydrogen on both sides of the membrane. The total pressure in the permeate side is set at 1 bar. In this work, an isotherm plug flow reactor is assumed to model this unit. The set of differential equations to describe the mass balances is as follows (S28-S30) (Sánchez and Martín, 2018):

$$\frac{dF_{NH_3}}{dz} = -Ar_{NH_3} \tag{S28}$$

$$\frac{dF_{N_2}}{dz} = \frac{1}{2} Ar_{NH_3} \tag{S29}$$

$$\frac{dF_{H_2}}{dz} = \frac{3}{2} A r_{NH_3} - L_{cir} r^p_{H_2} \tag{S30}$$

Where A is the cross-sectional area of the reactor, L_{cir} is the cross-sectional length of the membrane and F_i is the molar flowrate of component i. The activity of each species is computed using the expression S31.

$$a_i = y_i \gamma_i P \tag{S31}$$

The fugacity coefficients γ_i are calculated as a function of pressure and temperature using the correlations proposed by Dyson and Simon (1968). The kinetic constant (k_{reac}) is expressed as a function of the temperature according to equation S32.

$$k_{reac} = 8.849 \cdot 10^{14} \exp\left(\frac{-40765}{1.988T}\right) \tag{S32}$$

The thermodynamic equilibrium constant K_p is also computed as a function of the temperature of the reactor (Martín, 2016):

$$\log_{10}(K_p) = \frac{2250.322}{T} - 0.85430 - 1.51049 \log_{10}(T) - 2.58987 \cdot 10^{-4} T + 1.48961 \cdot 10^{-7} T^2 \tag{S33}$$

The initial velocity is an input parameter of this model. Based on this value, the cross-sectional area is calculated:

$$Q^0 = \frac{F_t^0}{\rho^0} \tag{S34}$$

$$\rho^0 = \frac{P^0}{RT} \tag{S35}$$

$$A = \frac{Q^0}{v^0} \tag{S36}$$

To compute the pressure drop in the catalytic side, the Ergun equation is introduced:

$$\frac{dP}{dz} = -150 \frac{(1-\varepsilon)^2}{\varepsilon^3} \frac{\mu \nu}{d_p^2} - 1.75 \frac{(1-\varepsilon)}{\varepsilon^3} \frac{\rho \nu^2}{d_p} \tag{S37}$$

3.2 Methanol catalytic bed reactor

Methanol is steam reformed in a catalytic fixed bed reactor to produce mainly hydrogen, but carbon monoxide and carbon dioxide are also produced according to the reactions S38-S39. The reaction S38 is the methanol steam reforming, the reaction S39 is the water gas shift reaction and the reaction S40 is the methanol decomposition reaction.

$$CH_3OH + H_2O \rightleftharpoons CO_2 + 3\,H_2 \tag{S38}$$

$$CO + H_2O \rightleftharpoons CO_2 + H_2 \tag{S39}$$

$$CH_3OH \rightleftharpoons CO + 2\,H_2 \tag{S40}$$

The catalyst used in the decomposition section is $Cu/ZnO/Al_2O_3$. As the limiting step is the adsorption of the reactants on the catalyst surface, the reaction mechanism is based on the Langmuir-Hinshelwood kinetic model and the kinetics expressions for each of the reactions are taken from the literature (Peppley et al., 1999) (S41-S43). It is noted that there are two different types of active centers: in type 1, the reforming and water gas reactions are carried out, and in type 2, the methanol decomposition reaction.

$$r_R = \frac{k_R K^*_{CH_3O(1)} \left(p_{CH_3OH}/p^{1/2}_{H_2}\right) \left(1 - p^3_{H_2} p_{CO_2}/K^{eq}_R p_{CH_3OH} p_{H_2O}\right) C^T_{S_1} C^T_{S_{1a}}}{\left(1 + K^*_{CH_3O(1)} \left(p_{CH_3OH}/p^{1/2}_{H_2}\right) + K^*_{HCOO(1)} p_{CO_2} p^{1/2}_{H_2} + K^*_{OH(1)} \left(p_{H_2O}/p^{1/2}_{H_2}\right)\right) \left(1 + K^{*1/2}_{H(1a)} p^{1/2}_{H_2}\right)} \tag{S41}$$

$$r_W = \frac{k^*_W K^*_{OH(1)} \left(p_{CO} p_{H_2O}/p^{1/2}_{H_2}\right) \left(1 - p_{H_2} p_{CO_2}/K^{eq}_W p_{CO} p_{H_2O}\right) C^{T^2}_{S_1}}{\left(1 + K^*_{CH_3O(1)} \left(p_{CH_3OH}/p^{1/2}_{H_2}\right) + K^*_{HCOO(1)} p_{CO_2} p^{1/2}_{H_2} + K^*_{OH(1)} \left(p_{H_2O}/p^{1/2}_{H_2}\right)\right)^2} \tag{S42}$$

$$r_D = \frac{k_D K^*_{CH_3O(2)} \left(p_{CH_3OH}/p^{1/2}_{H_2}\right) \left(1 - p^2_{H_2} p_{CO}/K^{eq}_D p_{CH_3OH}\right) C^T_{S_2} C^T_{S_2a}}{\left(1 + K^*_{CH_3O(2)} \left(p_{CH_3OH}/p^{1/2}_{H_2}\right) + K^*_{OH(2)} \left(p_{H2O}/p^{1/2}_{H_2}\right)\right) \left(1 + K^{*1/2}_{H(2a)} p^{1/2}_{H_2}\right)} \tag{S43}$$

Where $C^T_{S_i}$ is the total surface concentration of each site (1, 1a, 2 and 2a); k_j is the rate constant for reaction j (j = R, W, D); K^{eq}_j is the equilibrium constant of reaction j (j = R, W, D); p_i is the partial pressure of component i (i = CO_2, CO, H_2, CH_3OH and H_2O) and K^* the adsorption coefficient.

The values of the parameters required for the model are given in Table S1 and Table S2. The temperature dependence of each of the constants, from the Arrhenius equation, is given in Equations S44-S56 according to Zhu et al. (2020) and Peppley et al. (1999).

$$k_R = k^\infty_R \exp\left(\frac{-E_R}{RT}\right) \tag{S44}$$

$$k_D = k^\infty_D \exp\left(\frac{-E_D}{RT}\right) \tag{S45}$$

$$k_W = k^\infty_W \exp\left(\frac{-E_W}{RT}\right) \tag{S46}$$

$$K^{eq}_R = \exp\left(-\frac{50240 - 170.98T - 2.64 \cdot 10^{-2} T^2}{RT}\right) \tag{S47}$$

$$K^{eq}_W = \exp\left(-\frac{-41735 + 46.66T - 7.55 \cdot 10^{-3} T^2}{RT}\right) \tag{S48}$$

$$K^{eq}_D = \frac{K_R eq}{K^{eq}_W} \tag{S49}$$

$$K^*_{CH_3O(1)} = \exp\left(\frac{\Delta S^*_{CH_3O(1)}}{R} - \frac{\Delta H^*_{CH_3O(1)}}{RT}\right) \tag{S50}$$

$$K^*_{HCOO(1)} = \exp\left(\frac{\Delta S^*_{HCOO(1)}}{R} - \frac{\Delta H^*_{HCOO(1)}}{RT}\right) \tag{S51}$$

$$K^*_{OH(1)} = \exp\left(\frac{\Delta S^*_{OH(1)}}{R} - \frac{\Delta H^*_{OH(1)}}{RT}\right) \tag{S52}$$

$$K^*_{H(1)} = \exp\left(\frac{\Delta S^*_{H(1)}}{R} - \frac{\Delta H^*_{H(1)}}{RT}\right) \tag{S53}$$

$$K^*_{CH_3O(2)} = \exp\left(\frac{\Delta S^*_{CH_3O(2)}}{R} - \frac{\Delta H^*_{CH_3O(2)}}{RT}\right) \tag{S54}$$

$$K^*_{OH(2)} = \exp\left(\frac{\Delta S^*_{OH(2)}}{R} - \frac{\Delta H^*_{OH(2)}}{RT}\right) \tag{S55}$$

$$K^*_{H(2a)} = \exp\left(\frac{\Delta S^*_{H(2a)}}{R} - \frac{\Delta H^*_{H(2a)}}{RT}\right) \tag{S56}$$

Where R is the ideal gas constant, k_j^∞ is the pre-exponential term in Arrhenius expression of reaction j, E_j is the activation energy for rate constant of reaction j, T is the temperature, ΔS_i^* is the entropy of adsorption for species i and ΔH_i^* is the heat of adsorption for surface species i.

As in the case of ammonia, an isotherm plug flow reactor is assumed to model this unit. The set of differential equations to describe the mass balances is as follows (S57-S61) (Qureshi et al., 2021):

$$\frac{dF_{CH_3OH}}{dL} = \eta\pi r_{in}^2 \rho_B S\left(-r_R - r_D\right) \tag{S57}$$

$$\frac{dF_{H_2O}}{dL} = \eta\pi r_{in}^2 \rho_B S\left(-r_R - r_W\right) \tag{S58}$$

$$\frac{dF_{CO_2}}{dL} = \eta\pi r_{in}^2 \rho_B S\left(r_R + r_W\right) \tag{S59}$$

$$\frac{dF_{CO}}{dL} = \eta\pi r_{in}^2 \rho_B S\left(r_D - r_W\right) \tag{S60}$$

$$\frac{dF_{H_2}}{dL} = \eta\pi r_{in}^2 \rho_B S\left(3r_R + 2r_D + r_W\right) \tag{S61}$$

Where F_i is the molar flux for species i, r_{in} is the inner tube radius, ρ_B is the bulk density of the catalyst bed, S is the surface area per unit mass of fresh catalyst and r_j is the rate of production on reaction j.

Table S1: Parameter values of the kinetic model of methanol steam reforming on $Cu/ZnO/Al_2O_3$ (Peppley et al., 1999).

k_j (m^2 s^{-1} mol^{-1}) or K_j^{eq} ($atm^{-0.5}$)	ΔS_i^* (J mol^{-1} K^{-1}) or k_i^∞ (m^2 s^{-1} mol^{-1})	ΔH_i^* (J mol^{-1}) or E (J mol^{-1})
k_R	$7.4{\cdot}10^{14}$	102800
$K^*_{CH_3O^{(1)}}$	-41.8	-20000
$K^*_{OH^{(1)}}$	-44.5	-20000
$K^*_{H^{1a}}$	-100.8	-50000
$K^*_{HCOO^{(1)}}$	179.2	100000
k_D	$3.8{\cdot}10^{20}$	170000
$K^*_{CH_2O^{(2)}}$	30.0	-20000
$K^*_{OH^{(2)}}$	30.0	-20000
$K^*_{H^{2a}}$	-46.2	-50000
k_W	$5.9{\cdot}10^{13}$	87600

Table S2: Total concentration of active centers values (Peppley et al., 1999).

Total concentration of active centers (mol m^{-2})
$C^T_{S_1}$	$7.5{\cdot}10^{-6}$
$C^T_{S_{1a}}$	$1.5{\cdot}10^{-5}$
$C^T_{S_2}$	$7.5{\cdot}10^{-6}$
$C^T_{S_{2a}}$	$1.5{\cdot}10^{-5}$

4 NO_x concentration in the thermochemical route

It is important to evaluate this emissions in order to comply with the environmental restrictions. In the case of ammonia, the amount of NO_x leaving the facility is obtained as a function of the equivalent ratio (ER) (S63). This equivalent ratio is defined as the relation between the amount of oxygen fed into the gas turbine and the stoichiometric oxygen taking into account the reaction S62.

$$NH_3 + \frac{5}{4} O_2 \rightleftharpoons NO + \frac{3}{2} H_2O \tag{S62}$$

$$NO\ (ppm) = 2.9951 \cdot 10^{19} e^{-31.984 ER} \tag{S63}$$

In the case of methanol, the amount of NO_x is obtained from its mass fraction ($x_{m_{NO}}$) in the flue gases, which is calculated from the percentage of hydrogen fed into the gas turbine (Equation S64).

$$x_{m_{NO}} = 0.001 e^{14.99\%_{H_2}} \tag{S64}$$

5 Exergy Calculation Procedure

The overall exergy efficiency (ε) of the different alternatives has been evaluated, as shown in Equation S65 (Al-Hamed and Dincer, 2021).

$$\varepsilon = \frac{W}{\sum_j ex_{j_{in}}} \tag{S65}$$

Where W is the net power production of each alternative, and ex_{in} is the specific exergy of the inlet fuel. The vale of the specific exergy for each of the inlet streams of fuel (j) is calculated by adding up the specific physical exergy (ex_j^{ph}) and the specific chemical exergy (ex_j^{ch}) of the stream as follows (Eq.S66).

$$ex_j = ex_j^{ph} + ex_j^{ch} \tag{S66}$$

The specific physical exergy is defined in Equation S67, where T_0 is the reference temperature, h_j and s_j are the specific enthalpy and entrophy of the stream, respectively, evaluated at the temperature of the stream, and h_0 and s_0 are the specific enthalpy of the stream, respectively, evaluated at the reference temperature. The different values of specific entalphy and entrophy can be seen in Table S3.

$$ex_j^{ph} = (h_j - h_0) - T_0\,(s_j - s_0) \tag{S67}$$

The specific chemical exergy for stream mixtures is obtained following Equation S68, which is adopted from Cohce et al. (2011).

$$ex_j^{ch} = \sum_k x_k \left(ex_k^{ch,0} - R\,T\,ln(x_k) \right) \tag{S68}$$

where x_k is the molar ratio of the component k within the mixture, $ex_k^{ch,0}$ is the standard specific chemical exergy for the component and R is the gas constant. In this case, since only pure fuel is introduced into the process, the value of x_k is always 1 for each case, and the values of the specific chemical exergy are 720.0 kJ/mol and 337.9 kJ/mol for methanol and ammonia, respectively.

Table S3: Summary of the specific entalphies and entrophies for the inlet methanol and ammonia in the two different routes, termochemical and electrochemical.

Route	Stream	h_j (kJ/s)	h_0 (kJ/s)	s_j (kJ/K s)	s_0 (kJ/K s)
Termochemical	$NH_{3_{Src1-HX01}}$	-5364.8	-5385.8	-11.54	-11.61
Termochemical	$NH_{3_{Src6-M02}}$	-39086	-37423	-86.87	-80.67
Termochemical	$CH_3OH_{Src1-HX01}$	-98436.9	-98436.9	-104.3	-104.3
Electrochemical	$NH_{3_{Src1-S01}}$	-1448.7	-923.26	-4.16	-1.99
Electrochemical	$CH_3OH_{Src1-HX01}$	-4117.0	-4117.0	-1.502	-1.502

6 Cost Estimation Procedure

With the results obtained in the optimization procedure, the economic analysis is carried out. First, the capital cost is estimated based on the factorial method proposed by Sinnott (2005). The first step consists of calculating the total purchase cost of the major equipment of the facility. For the basic units such as heat exchangers or compressors, the cost is estimated based on the correlations proposed by Almena and Martín (2015), in both cases, thermochemical and electrochemical routes. In the case of ammonia decomposition reactor in the thermochemical way, the price of the Ni/Al_2O_3 is set at 30 €/kg (Jess and Wasserscheid, 2020) and the Pd/Ag supported membrane at 1500 €/m^2 (De Falco et al., 2011). In the case of the methanol steam reforming reactor, the price for $Cu/ZnO/Al_2O_3$ is also set at 30 €/kg (Lee et al., 2019). The costs of the gas and steam turbines, in both, ammonia and methanol, thermochemical routes, are calculated as a function of the produced power (Caputo et al., 2005). In the electrochemical route, the unit price per kW of generated power of the fuel cells is set at 1494 €/kW for ammonia fuel cells (EEPOWER, 2018) and at 1650 €/kW for methanol fuel cells (Sgroi et al., 2016). The SCR treatment consists, for ammonia thermochemical and electrochemical routes, of a fixed bed reactor with a GHSV equal to 8000 h^{-1} (Yu et al., 2010). The catalyst is Pd/Al_2O_3 with a price equal to 2501 €/kg (Pappaterra et al., 2021). With the total purchase cost of the major equipment, a detailed factorial estimation is applied to calculate the fixed capital of the facility including piping, instrumentation, erection, etc. For a facility working with fluids, the total factor is equal to 1.45 in both routes.

Operating cost is a sum of two terms: the fixed and variable costs (see Table S4). The fixed part includes maintenance, labor, capital charges, etc. and is estimated as a percentage of different items, as shown in Table S4. Labor costs are computed using the correlation proposed by Green and Perry (2007). The costs of the raw materials and utilities are also included. The price of ammonia is fixed to 0.55 €/kg (Matzen et al., 2015a) and the price of methanol, to 0.43 €/kg (Matzen et al., 2015a); however, the influence of the variation of this parameter is assessed in this work based on the different fuel production technologies. The price of argon, nitrogen and hydrogen are set at 0.037 €/kg (Elishav et al., 2017), 0.5 S.5 €/kg (Downie, 1996) and 4 €/kg (Matzen et al., 2015a), respectively. The cost of utilities are equal to 2.20 €/GJ

for steam (Yang and You, 2018), 4.58 €/kt (Yang and You, 2018) for cooling water and 0.0787 €/kWh (Statista, 2021) for electricity.

Table S4: Summary of the operating cost calculations (Sinnott, 2005).

Variable costs	
Raw materials	from flowsheet optimization
Miscellaneous materials	10% of Maintenance
Utilities	from flowsheet optimization
Fixed Costs	
Maitenance	5% of fixed capital
Labour	Estimated from correlations
Laboratory	20% of Labour
Supervision	20% of Labour
Plant Overheads	50% of Labour
Capital Charges	10% of fixed capital
Insurance	1% of fixed
Taxes	2% of fixed capital

7 Results

7.1 Energy performance

Firstly, in Figure S5, a Sankey diagram is presented to show the energy flows in the thermochemical process in which ammonia is used as fuel. Secondly, in Figure S6, a Sankey diagram is presented to show the energy flows in the thermochemical process in which methanol is used as fuel.

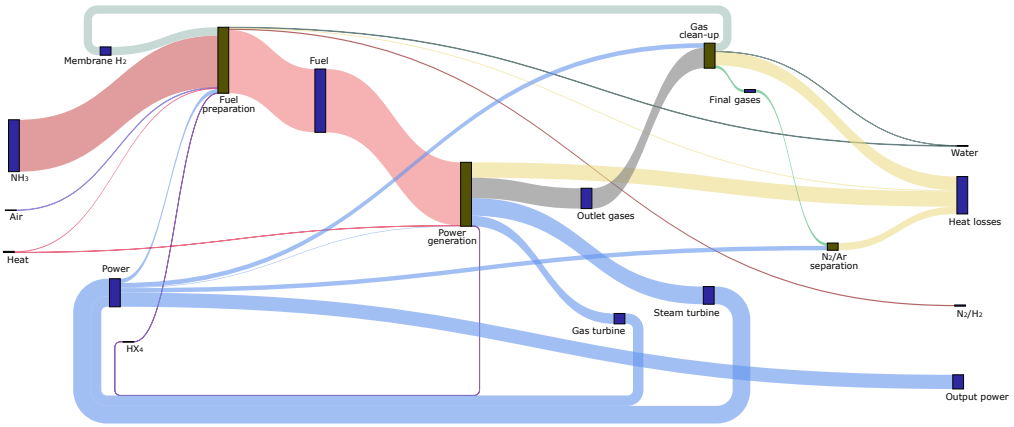

Figure S5: Energy flows for the process based on ammonia combustion.

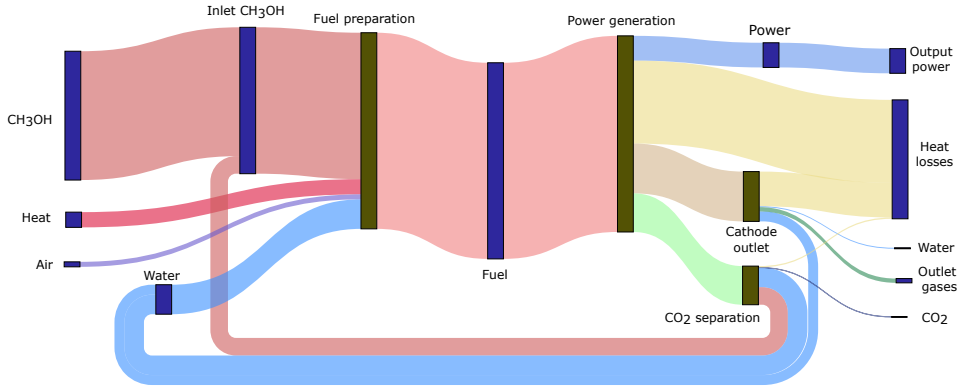

Figure S6: Energy flows for the process based electrochemical conversion of methanol.

7.2 Sensitivity analysis

Firstly, in Figure S7, the sensitivity analysis for the thermochemical conversion of ammonia is presented. Secondly, in Figure S8, the sensitivity analysis for the electrochemical conversion of methanol is presented.

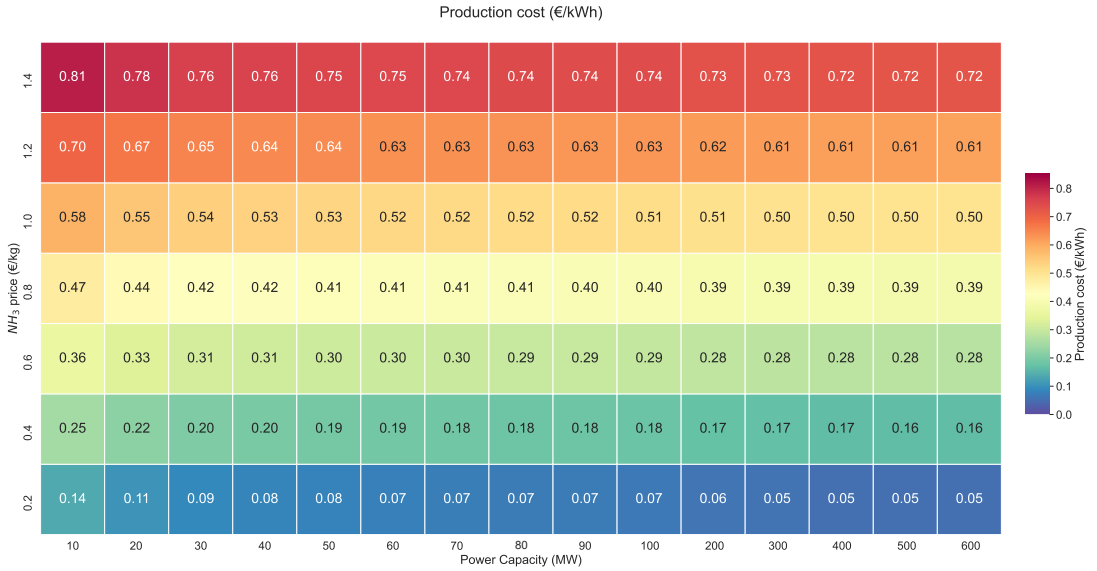

Figure S7: Cost of electricity via the termochemical conversion of ammonia for different ammonia prices and production capacities.

Figure S8: Cost of electricity via the electrochemical conversion of methanol for different methanol prices and production capacities.

References

Abashar, M., 2018. Ultra-clean hydrogen production by ammonia decomposition. Journal of King Saud University - Engineering Sciences 30, 2–11. URL: https://www.sciencedirect.com/science/article/pii/S1018363916000064, doi:https://doi.org/10.1016/j.jksues.2016.01.002.

Achrai, B., Zhao, Y., Wang, T., Tamir, G., Abbasi, R., Setzler, B.P., Page, M., Yan, Y., Gottesfeld, S., 2020. A direct ammonia fuel cell with a KOH-free anode feed generating 180 mW cm-2 at 120 °c. Journal of The Electrochemical Society 167, 134518. URL: https://doi.org/10.1149/1945-7111/abbdd1, doi:10.1149/1945-7111/abbdd1.

Al-Hamed, K.H., Dincer, I., 2021. A novel ammonia solid oxide fuel cell-based powering system with on-board hydrogen production for clean locomotives. Energy 220, 119771. URL: https://www.sciencedirect.com/science/article/pii/S0360544221000207, doi:https://doi.org/10.1016/j.energy.2021.119771.

Almena, A., Martín, M., 2015. Technoeconomic analysis of the production of epichlorohydrin from glycerol. Industrial & Engineering Chemistry Research 55. doi:10.1021/acs.iecr.5b02555.

Caputo, A.C., Palumbo, M., Pelagagge, P.M., Scacchia, F., 2005. Economics of biomass energy utilization in combustion and gasification plants: effects of logistic variables. Biomass and Bioenergy 28, 35–51. URL: https://www.sciencedirect.com/science/article/pii/S0961953404001205, doi:https://doi.org/10.1016/j.biombioe.2004.04.009.

Cechetto, V., Di Felice, L., Medrano, J.A., Makhloufi, C., Zuniga, J., Gallucci, F., 2021. H2 production via ammonia decomposition in a catalytic membrane reactor. Fuel Processing Technology 216, 106772. URL: https://www.sciencedirect.com/science/article/pii/S0378382021000515, doi:https://doi.org/10.1016/j.fuproc.2021.106772.

Cha, S.W., O'Hayre, R., Colella, W., Prinz, F., 2009. Fuel Cell Fundamentals.

Chiuta, S., Everson, R.C., Neomagus, H.W., van der Gryp, P., Bessarabov, D.G., 2013. Reactor technology options for distributed hydrogen generation via ammonia decomposition: A review. International Journal of Hydrogen Energy 38, 14968 – 14991. URL: http://www.sciencedirect.com/science/article/pii/S0360319913022908, doi:https://doi.org/10.1016/j.ijhydene.2013.09.067.

Cohce, M., Dincer, I., Rosen, M., 2011. Energy and exergy analyses of a biomass-based hydrogen production system. Bioresource Technology 102, 8466–8474. URL: https://www.sciencedirect.com/science/article/pii/S0960852411008236, doi:https://doi.org/10.1016/j.biortech.2011.06.020.

De Falco, M., Marrelli, L., Iaquaniello, G., 2011. Membrane Reactors for Hydrogen Production Processes. Springer London. URL: https://books.google.es/books?id=-g2huAO89aQC.

Dincer, I., Siddiqui, O., 2020. Chapter 4 - ammonia fuel cells, in: Dincer, I., Siddiqui, O. (Eds.), Ammonia Fuel Cells. Elsevier, pp. 77–122. URL: https://www.sciencedirect.com/science/article/pii/B9780128228258000049, doi:https://doi.org/10.1016/B978-0-12-822825-8.00004-9.

Downie, N., 1996. Industrial Gases. Springer Netherlands. URL: https://books.google.co.cr/books?id=1EZ7GF3NEr0C.

Downie, N.A., 2007. Industrial gases. Springer Science & Business Media.

Duynslaegher, C., Jeanmart, H., Vandooren, J., 2009. Flame structure studies of premixed ammonia/hydrogen/oxygen/argon flames: Experimental and numerical investigation. Proceedings of the Combustion Institute 32, 1277–1284. URL: https://www.sciencedirect.com/science/article/pii/S1540748908000801, doi:https://doi.org/10.1016/j.proci.2008.06.036.

Dyson, D.C., Simon, J.M., 1968. Kinetic expression with diffusion correction for ammonia synthesis on industrial catalyst. Industrial & Engineering Chemistry Fundamentals 7, 605–610. URL: https://doi.org/10.1021/i160028a013, doi:10.1021/i160028a013, arXiv:https://doi.org/10.1021/i160028a013.

EEPOWER, 2018. Ammonia fuel cell is cost competitive with diesel generators. URL: https://eepower.com/new-industry-products/ammonia-fuel-cell-is-cost-competitive-with-diesel-generators/#.

Elishav, O., Tvil, G., Mosevitzky, B., Lewin, D., Shter, G.E., Grader, G.S., 2017. The nitrogen economy: The feasibility of using nitrogen-based alternative fuels. Energy Procedia 135, 3–13. URL: https://www.sciencedirect.com/science/article/pii/S187661021734585X, doi:https://doi.org/10.1016/j.egypro.2017.09.482. 11th International Renewable Energy Storage Conference, IRES 2017, 14-16 March 2017, Düsseldorf, Germany.

Ghasemzadeh, K., Harasi, J., Amiri, T., Basile, A., Iulianelli, A., 2020. Methanol steam reforming for hydrogen generation: A comparative modeling study between silica and pd-based membrane reactors by cfd method. Fuel Processing Technology 199, 106273. URL: https://www.sciencedirect.com/science/article/pii/S0378382019317965, doi:https://doi.org/10.1016/j.fuproc.2019.106273.

Gong, C., Li, D., Li, Z., Liu, F., 2016. Numerical study on combustion and emission in a disi methanol engine with hydrogen addition. International Journal of Hydrogen Energy 41, 647–655. URL: https://www.sciencedirect.com/science/article/pii/S0360319915302044, doi:https://doi.org/10.1016/j.ijhydene.2015.11.062.

Green, D., Perry, R., 2007. Perry's Chemical Engineers' Handbook, Eighth Edition. McGraw Hill professional, McGraw-Hill Education. URL: https://books.google.es/books?id=tH7IVcA-MX0C.

Guerras, L.S., Martín, M., 2019. Optimal gas treatment and coal blending for reduced emissions in power plants: A case study in northwest spain. Energy 169, 739–749. URL: https://www.sciencedirect.com/science/article/pii/S0360544218324551, doi:https://doi.org/10.1016/j.energy.2018.12.089.

Jess, A., Wasserscheid, P., 2020. Chemical Technology: From Principles to Products. Wiley. URL: https://books.google.es/books?id=a97BDwAAQBAJ.

Khateeb, A.A., Guiberti, T.F., Zhu, X., Younes, M., Jamal, A., Roberts, W.L., 2020. Stability limits and no emissions of technically-premixed ammonia-hydrogen-nitrogen-air swirl flames. International Journal of Hydrogen Energy 45, 22008 – 22018. URL: http://www.sciencedirect.com/science/article/pii/S0360319920320917, doi:https://doi.org/10.1016/j.ijhydene.2020.05.236.

Kim, S., Song, J., Lim, H., 2018. Conceptual feasibility studies of a cox-free hydrogen production from ammonia decomposition in a membrane reactor for pem fuel cells. Korean Journal of Chemical Engineering 35. doi:10.1007/s11814-018-0037-5.

Lee, J., Lee, S., Han, D., Gwak, G., Ju, H., 2017. Numerical modeling and simulations of active direct methanol fuel cell (dmfc) systems under various ambient temperatures and operating conditions. International Journal of Hydrogen Energy 42, 1736–1750. URL: https://www.sciencedirect.com/science/article/pii/S036031991631120X, doi:https://doi.org/10.1016/j.ijhydene.2016.09.087. the 6th European Fuel Cell Technology & Applications Piero Lunghi Conference & Exhibition (EFC15), 16-18 December 2015, Naples, Italy.

Lee, J.K., Lee, I.B., Han, J., 2019. Techno-economic analysis of methanol production from joint feedstock of coke oven gas and basic oxygen furnace gas from steel-making. Journal of Industrial and Engineering Chemistry 75, 77–85. URL: https://www.sciencedirect.com/science/article/pii/S1226086X19300681, doi:https://doi.org/10.1016/j.jiec.2019.02.019.

León, E., Martín, M., 2016. Optimal production of power in a combined cycle from manure based biogas. Energy Conversion and Management 114, 89 – 99. URL: http://www.sciencedirect.com/science/article/pii/S0196890416300255, doi:https://doi.org/10.1016/j.enconman.2016.02.002.

Li, X., Faghri, A., 2013. Review and advances of direct methanol fuel cells (dmfcs) part i: Design, fabrication, and testing with high concentration methanol solutions. Journal of Power Sources 226, 223–240. URL: https://www.sciencedirect.com/science/article/pii/S0378775312016175, doi:https://doi.org/10.1016/j.jpowsour.2012.10.061.

Martín, M.M., 2016. Chapter 5 - syngas, in: Martín, M.M. (Ed.), Industrial Chemical Process Analysis and Design. Elsevier, Boston, pp. 199–297. URL: https://www.sciencedirect.com/science/article/pii/B9780081010938000057, doi:https://doi.org/10.1016/B978-0-08-101093-8.00005-7.

Matzen, M., Alhajji, M., Demirel, Y., 2015a. Chemical storage of wind energy by renewable methanol production: Feasibility analysis using a multi-criteria decision matrix. Energy 93, 343 – 353. URL: http://www.sciencedirect.com/science/article/pii/S0360544215012530, doi:https://doi.org/10.1016/j.energy.2015.09.043.

Matzen, M.J., Alhajji, M.H., Demirel, Y., 2015b. Technoeconomics and sustainability of renewable methanol and ammonia productions using wind power-based hydrogen. Journal of Advanced Chemical Engineering 3, 10100128.

Na, Y., Zenith, F., Krewer, U., 2015. Increasing fuel efficiency of direct methanol fuel cell systems with feedforward control of the operating concentration. Energies 8, 10409–10429. URL: https://www.mdpi.com/1996-1073/8/9/10409, doi:10.3390/en80910409.

Pappaterra, M., Xu, P., van der Meer, W., Faria, J.A., Fernandez Rivas, D., 2021. Cavitation intensifying bags improve ultrasonic advanced oxidation with pd/al2o3 catalyst. Ultrasonics Sonochemistry 70, 105324. URL: https://www.sciencedirect.com/science/article/pii/S1350417720305770, doi:https://doi.org/10.1016/j.ultsonch.2020.105324.

Peppley, B.A., Amphlett, J.C., Kearns, L.M., Mann, R.F., 1999. Methanol–steam reforming on cu/zno/al2o3 catalysts. part 2. a comprehensive kinetic model. Applied Catalysis A: General 179, 31–49. URL: https://www.sciencedirect.com/science/article/pii/S0926860X98002993, doi:https://doi.org/10.1016/S0926-860X(98)00299-3.

Qureshi, F., Ahmad, F., Idrees, M., Khan, A.A., Zaidi, S., 2021. Simulation of methanol steam reforming process for the production of hydrogen. Indian Chemical Engineer 63, 99–116. URL: https://doi.org/10.1080/00194506.2019.1689186, doi:10.1080/00194506.2019.1689186, arXiv:https://doi.org/10.1080/00194506.2019.1689186.

Sadi, M., Arabkoohsar, A., 2019. Exergoeconomic analysis of a combined solar-waste driven power plant. Renewable Energy 141, 883 – 893. URL: http://www.sciencedirect.com/science/article/pii/S0960148119305543, doi:https://doi.org/10.1016/j.renene.2019.04.070.

Schulze Lohoff, A., Kimiaie, N., Blum, L., 2016. The application of design of experiments and response surface methodology to the characterization of a direct methanol fuel cell stack. International Journal of Hydrogen Energy 41, 12222–12230. URL: https://www.sciencedirect.com/science/article/pii/S0360319915300914, doi:https://doi.org/10.1016/j.ijhydene.2016.05.248.

Sgroi, M.F., Zedde, F., Barbera, O., Stassi, A., Sebastián, D., Lufrano, F., Baglio, V., Aricò, A.S., Bonde, J.L., Schuster, M., 2016. Cost analysis of direct methanol fuel cell stacks for mass production. Energies 9. URL: https://www.mdpi.com/1996-1073/9/12/1008, doi:10.3390/en9121008.

Siddiqui, O., Dincer, I., 2019. Development and performance evaluation of a direct ammonia fuel cell stack. Chemical Engineering Science 200, 285–293. URL: https://www.sciencedirect.com/science/article/pii/S0009250919301538, doi:https://doi.org/10.1016/j.ces.2019.01.059.

Sinnott, R.K., 2005. Coulson and Richardson's chemical engineering. Vol. 6, Chemical engineering design. Fourth edition. ed., Elsevier Butterworth-Heinemann, Oxford.

Statista, 2021. Prices of electricity for the industry in spain from 2008 to 2018. URL: https://www.statista.com/statistics/595813/electricity-industry-price-spain/.

Sánchez, A., Castellano, E., Martín, M., Vega, P., 2021. Evaluating ammonia as green fuel for power generation: A thermo-chemical perspective. Applied Energy 293, 116956. URL: https://www.sciencedirect.com/science/article/pii/S0306261921004323, doi:https://doi.org/10.1016/j.apenergy.2021.116956.

Sánchez, A., Martín, M., 2018. Optimal renewable production of ammonia from water and air. Journal of Cleaner Production 178, 325–342. URL: https://www.sciencedirect.com/science/article/pii/S0959652617332730, doi:https://doi.org/10.1016/j.jclepro.2017.12.279.

Valera-Medina, A., Gutesa, M., Xiao, H., Pugh, D., Giles, A., Goktepe, B., Marsh, R., Bowen, P., 2019. Premixed ammonia/hydrogen swirl combustion under rich fuel conditions for gas turbines operation. International Journal of Hydrogen Energy 44, 8615 – 8626. URL: http://www.sciencedirect.com/science/article/pii/S0360319919305907, doi:https://doi.org/10.1016/j.ijhydene.2019.02.041.

Yang, M., You, F., 2018. Modular methanol manufacturing from shale gas: Techno-economic and environmental analyses of conventional large-scale production versus small-scale distributed, modular processing. Aiche Journal 64, 495–510.

Yu, Q., Kong, F., Li, L., Wu, G., Guan, N., 2010. Fast catalytic reduction of nox by h2 over pd-based catalysts. Chinese Journal of Catalysis 31, 261–263. URL: https://www.sciencedirect.com/science/article/pii/S1872206709600450, doi:https://doi.org/10.1016/S1872-2067(09)60045-0.

Yürüm, Y., 2013. Hydrogen Energy System: Production and Utilization of Hydrogen and Future Aspects. Nato Science Series E:, Springer Netherlands. URL: https://books.google.co.cr/books?id=bZQOswEACAAJ.

Zenith, F., Krewer, U., 2010. Modelling, dynamics and control of a portable dmfc system. Journal of Process Control 20, 630–642. URL: https://www.sciencedirect.com/science/article/pii/S0959152410000624, doi:https://doi.org/10.1016/j.jprocont.2010.02.014.

Zhang, B., Ji, C., Wang, S., 2015. Combustion analysis and emissions characteristics of a hydrogen-blended methanol engine at various spark timings. International Journal of Hydrogen Energy 40, 4707–4716. URL: https://www.sciencedirect.com/science/article/pii/S0360319915002347, doi:https://doi.org/10.1016/j.ijhydene.2015.01.142.

Zhang, J., Liu, H., 2009. Electrocatalysis of direct methanol fuel cells : from fundamentals to applications. Weinheim, Germany : Wiley-VCH ; Chichester : John Wiley [distributor]. URL: http://www.loc.gov/catdir/enhancements/fy1006/2010286596-t.html. formerly CIP.

Zhen, X., Wang, Y., 2015. An overview of methanol as an internal combustion engine fuel. Renewable and Sustainable Energy Reviews 52, 477–493. URL: https://www.sciencedirect.com/science/article/pii/S1364032115007303, doi:https://doi.org/10.1016/j.rser.2015.07.083.

Zhu, J., Araya, S.S., Cui, X., Sahlin, S.L., Kær, S.K., 2020. Modeling and design of a multi-tubular packed-bed reactor for methanol steam reforming over a cu/zno/al2o3 catalyst. Energies 13. URL: https://www.mdpi.com/1996-1073/13/3/610, doi:10.3390/en13030610.

Zhu, J., Meng, X., Zhao, J., Jin, Y., Yang, N., Zhang, S., Sunarso, J., Liu, S., 2017. Facile hydrogen/nitrogen separation through graphene oxide membranes supported on ysz ceramic hollow fibers. Journal of Membrane Science 535, 143 – 150. URL: http://www.sciencedirect.com/science/article/pii/S037673881730234X, doi:https://doi.org/10.1016/j.memsci.2017.04.032.